Progress in Medical Devices
ISSN: 2957-5478

Zentime

Research Article https://doi.org/10.61189/392182sdzooq

Optimal design and experimental study of Mg alloy electrodes for tissue welding

Juxiao Wang, Lin Mao, Weiwei Fan, Chengli Song

Shanghai Institute for Minimally Invasive Therapy, School of Health Science and Engineering, University of Shanghai for Science and Technology, Shanghai 200093, China.

Corresponding author: Lin Mao.

Declaration of conflict of interest: None.

Received December 31, 2024; Accepted February 19, 2025; Published March 31, 2025

Highlights

- Three types of circular electrodes with varying thicknesses were designed to achieve weight reduction, accompanied by support structures for intestinal tissue on both sides.
- The mechanical properties of the three electrode configurations were systematically compared to determine the optimal thickness for welding.
- In vitro tissue experiments successfully welded the tissue, identifying the optimal welding parameters.

Abstract

Objective: To investigate electrode weight reduction through structural modifications, focusing on variations in the thickness of circular electrodes to meet mechanical requirements. Additionally, optimal welding parameters were identified via experimental methods. **Methods:** Three electrode thicknesses were designed: 0.2 mm (T1), 0.3 mm (T2), and 0.4 mm (T3). The finite element method was used to analyze the stress, strain, and thermal effects on the surrounding tissue. In vitro tissue experiments assessed the mechanical strength of the anastomosis by measuring tear force and rupture pressure. **Results:** Among the three designs, the T3 electrode exhibited the lowest strain (1.2%) and stress (122.26 MPa). Thermal simulations showed maximum tissue damage of 53.3% and minimum damage of 48.6%. The maximum tear force (9.87±0.83 N) and rupture pressure (222.88±13.48 mmHg) were achieved with a compression force of 20 N, welding power of 160 W, and welding time of 8 seconds. **Conclusion:** T3 electrode demonstrated superior mechanical performance in the finite element analysis and successfully completed in vitro welding while minimizing electrode weight. Optimal welding parameters were identified.

Keywords: Radiofrequency tissue welding, electrode structure, finite element simulation, anastomosis strength

Introduction

Colorectal cancer has become the fourth leading cause of cancer-related mortality worldwide, accounting for approximately 900,000 deaths annually. In my country, it ranks as one of the most common malignancies of the digestive tract, with incidence and mortality rates placing third and fifth, respectively, among all cancers [1, 2]. Currently, the standard treatment involves surgical resection of the affected intestinal tissue, followed by anastomosis of the remaining stump [3]. Common methods for anastomosis include manual suturing and stapler anastomosis [4]. However, sutures and staples used in manual methods can remain in the body, potentially causing foreign body reactions. Additionally, complications such as bleeding and anastomotic fistula may arise from the procedure [5-7].

To improve the quality of intestinal tissue anastomosis, radiofrequency-based tissue welding technology has been proposed. This method uses a high-frequency current ranging from 300 to 500 kHz, which, under the combined influence of radiofrequency energy and mechanical pressure, generates heat through bioimpedance. This thermal effect denatures proteins in the intestinal tissue, leading to the formation of adhesions and the rapid creation of a continuous anastomosis [8, 9]. The technology offers several advantages, including a reduced risk of tissue infection, high suturing efficiency, no

Address correspondence to: Lin Mao, Shanghai Institute for Minimally Invasive Therapy, School of Health Science and Engineering, NO.516 Jungong Road, Shanghai 200093, China. Tel: +86-21-55572159. E-mail: linmao@usst.edu.cn.

Table 1. Electrode material properties

Name	Density, ρ (Kg/m^3)	Young's modulus (MPa)	Poisson ratio	YS (MPa)	UTS (MPa)	Thermal conductivity, λ (W/m/K)
WE43 magnesium alloy	1,866	45,270	0.27	162	250	51.3
Copper alloy	8,960	1.25e7	0.345	33.5	152	400

Note: YS, Yield strength; UTS, Ultimate tensile strength.

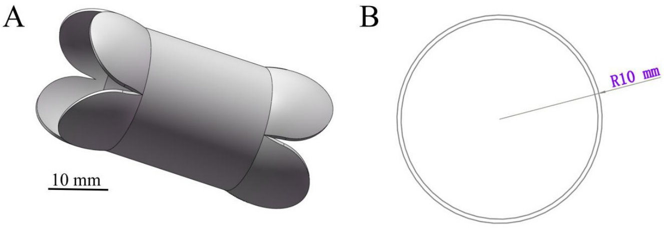

Figure 1. Overall electrode structure and thickness variations. (A) Overall electrode design; (B) Side view of the welding area with three different thicknesses (0.2 mm, 0.3 mm, 0.4 mm).

foreign material residue, and ease of operation [10].

Over the years, tissue welding technology based on radio frequency has seen significant advancements. In the late 1990s, the Ukrainian Paton Institute first proposed the use of radiofrequency currents for tissue welding [11]. Holmer et al. later confirmed that dual-electrode radiofrequency welding is an innovative method for achieving intestinal tissue anastomosis [12]. Zhao et al. used copper as the electrode material, designing two different electrode structures for intestinal tissue anastomosis [13]; however, the need for a second operation to remove the copper electrode impeded recovery. This led to the development of implantable electrodes as a preferred option for welding applications. Zong et al. were the first to use degradable magnesium alloys as welding electrodes for intestinal tissue anastomosis [14]. Mao et al. improved welding strength and reduced thermal damage by optimizing the structure of magnesium alloy electrodes, though they did not address concerns regarding in vivo fixation and electrode weight [15].

As electrodes used in tissue welding remain in the human body for extended periods, excessive electrode weight can negatively impact the subsequent recovery of intestinal tissue [16]. This study aims to investigate methods for reducing electrode weight. Three circular electrode designs with varying thicknesses were developed, incorporating support structures for the intestinal tissue on both sides. These structures were intended to enhance tissue fixation during the welding process and provide support to the anastomotic area during the healing phase. The forces acting on the electrodes were analyzed through a combined force-electrothermal simulation, and temperature variations at the anastomosis, along with the extent of thermal damage to the tissue, were assessed. Furthermore, optimal welding parameters were identified through in vitro tissue welding experiments, and the effects of different output powers on tissue pathological changes were evaluated. These findings lay the groundwork for future in vivo studies.

Materials and methods

Electrode structure design

The electrode structure consists of two main components: the central region, designated for welding intestinal tissue, and two end sections, which support the tissue and generate friction to prevent tissue retraction. The overall design of the electrode is shown in **Figure 1A**. To minimize electrode weight while evaluating their pressure resistance limits, three circular ring electrodes with varying thicknesses-0.2 mm, 0.3 mm, and 0.4 mm-were designed (**Figure 1B**). The thickness of the central region is consistent with that of the end sections across all three electrodes. Each electrode has an outer diameter of 20 mm, a length of 20 mm, and inner diameters of 19.6 mm, 19.4 mm, and 19.2 mm, respectively. The supporting structures at both ends are symmetrical, with a single-side length of 10 mm.

Electrode material characteristics

The outer electrode in the experiment was made of copper, which is known for its excellent electrical conductivity, thermal conductivity, and antibacterial properties [17]. The inner electrode was constructed from a WE43 magnesium alloy, designed to remain in the body following the welding process. The WE43 alloy is commercially available and is recognized for its good biocompatibility and ability to degrade gradually during the recovery of intestinal tissue [18]. The material properties of both electrodes are summarized in **Table 1** [19-21].

Mechanical simulation

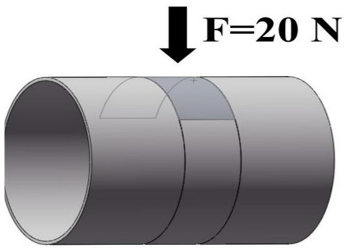

Figure 2. Force loading schematic.

Since the electrode primarily applies force to the central region during the welding process, the simulation model was simplified by excluding the support area. To accurately model the force distribution, the outermost surface of the central section of the electrode was divided into two regions: one-third and two-thirds of the circumference.

The mechanical analysis of the three electrodes was performed using ANSYS 2020 R2 software. After defining the boundary conditions for the finite element model, it was noted that the external copper electrode contacts only the middle third of the inner electrode (indicated by the dark region). Based on the force values from the corresponding experimental study, a 20 N force was applied to the middle third of the electrode, as shown in **Figure 2** [22].

Electrothermal simulation

The welding process was simulated using COMSOL 5.6 software. Since the support area is not involved in the welding region, it was excluded from the simulation model. As biological tissues were involved, the Pennies bioheat transfer model was applied. The governing equation for this model was:

$$\rho c \frac{\partial T}{\partial t} = \nabla \cdot (k \nabla T) + \rho_b c_b \omega (T_b - T) + Q \quad (1)$$

where ρ was the tissue density, c denoted the specific heat, k indicated the thermal conductivity, and T is the temperature. Additionally, ρ_b referred to blood density, c_b was the specific heat of blood, T_b represented arterial temperature, ω was the blood perfusion rate, and Q denoted the power absorption. Tissue thermal damage was calculated using the Arrhenius equation:

$$\Omega(\tau) = \int_0^{\tau} A e^{\frac{-E_a}{RT}} dt \quad (2)$$

where $\Omega(\tau)$ represented the degree of tissue damage, τ was the heating time, A denoted the frequency factor, E_a was the activation energy, R representd the molar gas constant, and T was the absolute temperature.

RF AC voltages of 120 W, 140 W, and 160 W were applied to the outer copper electrode, while zero voltage was applied to the inner magnesium electrode. The total simulation duration was 10 seconds, and the ambient temperature was set to 25 °C at t=0.

In vitro tissue welding experiment

Fresh porcine small intestines were obtained from a local slaughterhouse, rinsed briefly with 0.9% saline, and sectioned into 60-70 mm pieces. These were stored in phosphate buffer to maintain freshness and moisture. The LigaSure vascular sealing system (Valleylab, Covidien, USA) was used to supply radiofrequency power for tissue fusion. The intestinal tissue was placed on the surface of the magnesium alloy electrode (**Figure 3B**) in a mucosal-serosa orientation. The copper electrode applied pressure to the tissue, with pressure monitored using a gauge. A schematic of the welding experiment setup is shown in **Figure 3A**. Nine welding groups were designed with varying welding times and power levels, each replicated five times. Details of the experimental groups are outlined in **Table 2**.

Anastomosis strength test

The strength of the anastomosis was assessed using avulsion force and burst pressure tests. The avulsion force refers to the maximum tensile force applied to the anastomosis until it ruptured during stretching, while burst pressure referred to the maximum pressure at which the anastomosis began to leak during perfusion. For the tensile force test, the ends of the anastomotic tissue were secured in clamps of a universal material testing machine, and the tissue was stretched at a rate of 10 mm/s [15]. The tensile force at rupture was recorded (**Figure 3D**). For the burst pressure test, 0.9% saline was injected into the welded intestinal tissue at a constant rate of 2 ml/min, with the pressure value noted when leakage occurred from the anastomotic area (**Figure 3C**) [23].

Histopathological examination

Intestinal tissue samples, both pre- and post-welding, were collected and preserved in a neutral formalin solution. Histopathological examination was performed using a fluorescence microscope following standard procedures, including dehydration, clarification, paraffin em-

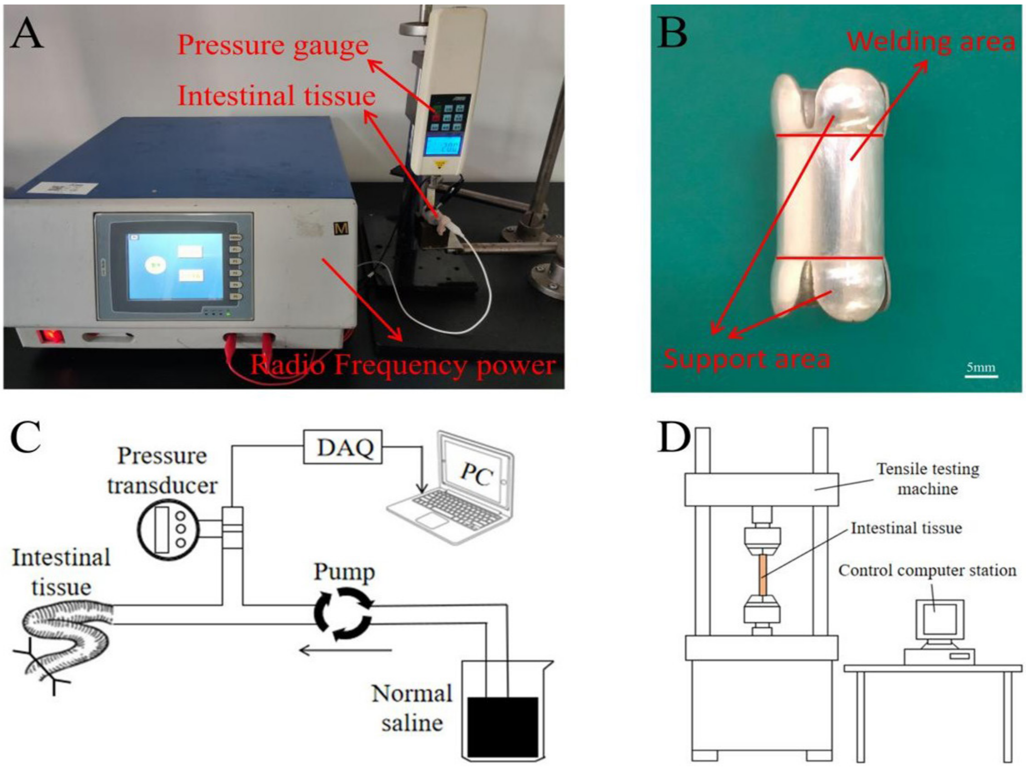

Figure 3. Experimental tissue welding in vitro. (A) Intestinal tissue welding platform; (B) WE43 magnesium alloy electrode; (C) Schematic diagram of burst pressure test; (D) Schematic diagram of avulsion force test. DAQ, Data acquisition card; PC, Personal computer.

Table 2. Welding experiments of each group

Group	Welding time (s)	Energy power (W)
1	6	120
2	8	
3	10	
4	6	140
5	8	
6	10	
7	6	160
8	8	
9	10	

bedding, sectioning, baking, hematoxylin-eosin staining, and neutral resin mounting.

Results

Electrode mechanics simulation results

A pressure of 20 N was applied to the circular electrode, and the strain distribution results are shown in **Figure 4A-C**. Under this pressure, the maximum deformations for the T1, T2, and T3 electrodes were 1.8903 mm, 0.5526 mm, and 0.2319 mm, respectively, with corresponding maximum strains of 9.2%, 2.8%, and 1.2%. The T3 electrode exhibited the smallest deformation, while the T1 electrode showed the largest. The maximum strains for all three electrodes occurred at the pressure application point, and the deformation decreased with increasing electrode thickness. All three electrodes were made of WE43 magnesium alloy, a material with an elongation range of 4% to 8% [24]. The strain in the T1 electrode (9.2%) exceeded the material's elongation limit, suggesting that fracture deformation would occur under the applied 20 N pressure. In contrast, the strains in the T2 (2.8%) and T3 (1.2%) electrodes remained below the material's elongation limit. Therefore, while the T1 electrode did not meet mechanical requirements due to excessive strain, the T2 and T3 electrodes exhibited strains within the allowable range, indicating they would meet the mechanical demands of the welding experiment.

The stress simulation results are presented in **Figure 4D-F**. Under a pressure of 20 N, the maximum stresses for the T1, T2, and T3 electrodes were 321.91 MPa, 181.43 MPa, and 122.26 MPa, respectively. The T3 electrode exhibited the lowest stress, while the T1 electrode experienced the highest. Additionally, stress in the electrode decreased with increasing electrode thickness. The yield strength of WE43 magnesium alloy is approximately 180-260 MPa [24]. The stresses in the T1 (321.91 MPa) and T2 (181.43 MPa) electrodes exceed the yield strength of the WE43 magnesium alloy,

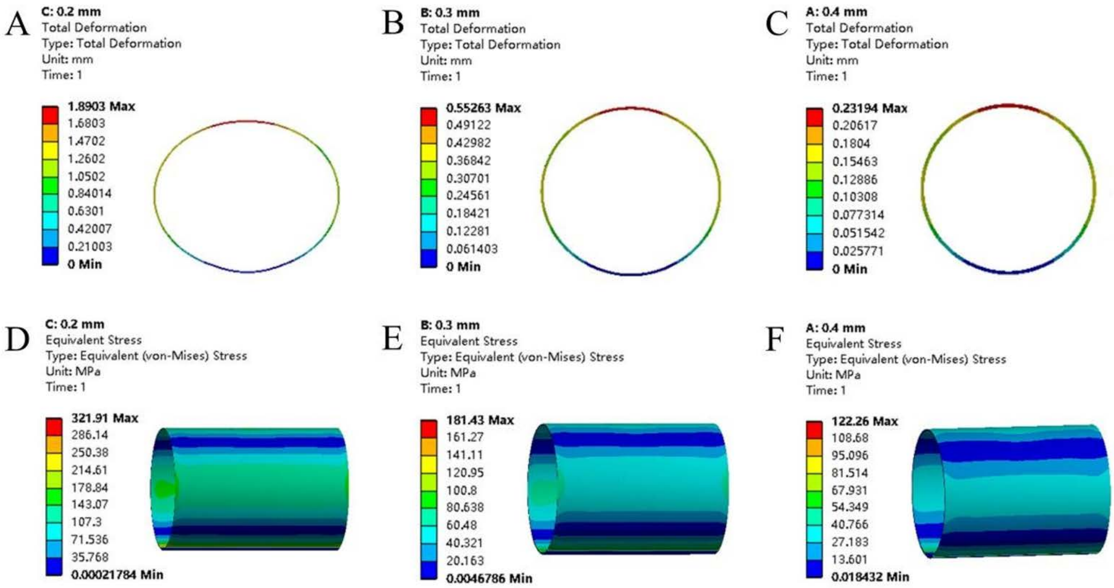

Figure 4. Mechanical simulation results of electrodes with different thicknesses (0.2 mm, 0.3 mm, 0.4 mm). (A-C) Simulation results of three types of electrode strain; (D-F) Simulation results of three types of electrode stress.

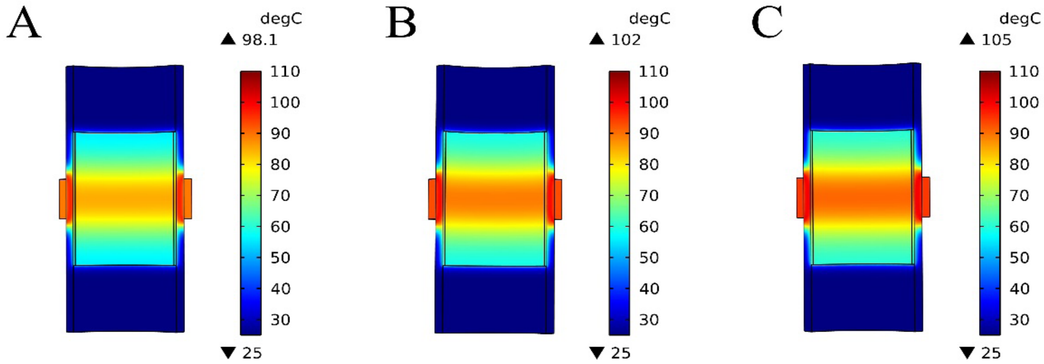

Figure 5. Electrothermal simulation results at different powers. (A) 120 W; (B) 140 W; (C) 160 W.

suggesting both electrodes would undergo plastic deformation, resulting in irreversible shape changes. From a stress perspective, the T1 and T2 electrodes cannot withstand the applied force during the experiment, while the T3 electrode satisfies the mechanical requirements.

Electrothermal simulation results

The temperature distribution of intestinal tissue at different power levels is illustrated in **Figure 5A-C**. As the power increases, the maximum temperature within the model also rises. The figure showed that the high-temperature region was primarily concentrated under the copper electrode, with the extent of the high-temperature area expanding as power increased. As seen in **Figure 6B**, the average maximum tissue temperatures at three different power levels were 65.1 °C, 68.0 °C, and 69.6 °C, respectively. All of these temperatures exceed 60 °C, indicating that successful welding can be achieved. Thermal damage to the tissue, shown in **Figure 6D**, begins to appear three seconds after power is applied and increases rapidly. After four seconds, the thermal damage area starts to expand gradually. At the three power levels, the average maximum thermal damage to the tissue was 48.6%, 51.6%, and 53.3%, respectively.

Additionally, two points, labeled a and b, were marked at the center and edge of the inner electrode (**Figure 6A**) to monitor temperature changes at different tissue sites. As shown in **Figure 6C**, the temperature at point b was significantly lower than at point a. The temperature at point a rose rapidly at first, then increased more slowly, while the temperature at point b increased steadily and gradually.

Biomechanical properties of anastomosis

In this experiment, the T3 electrode was used

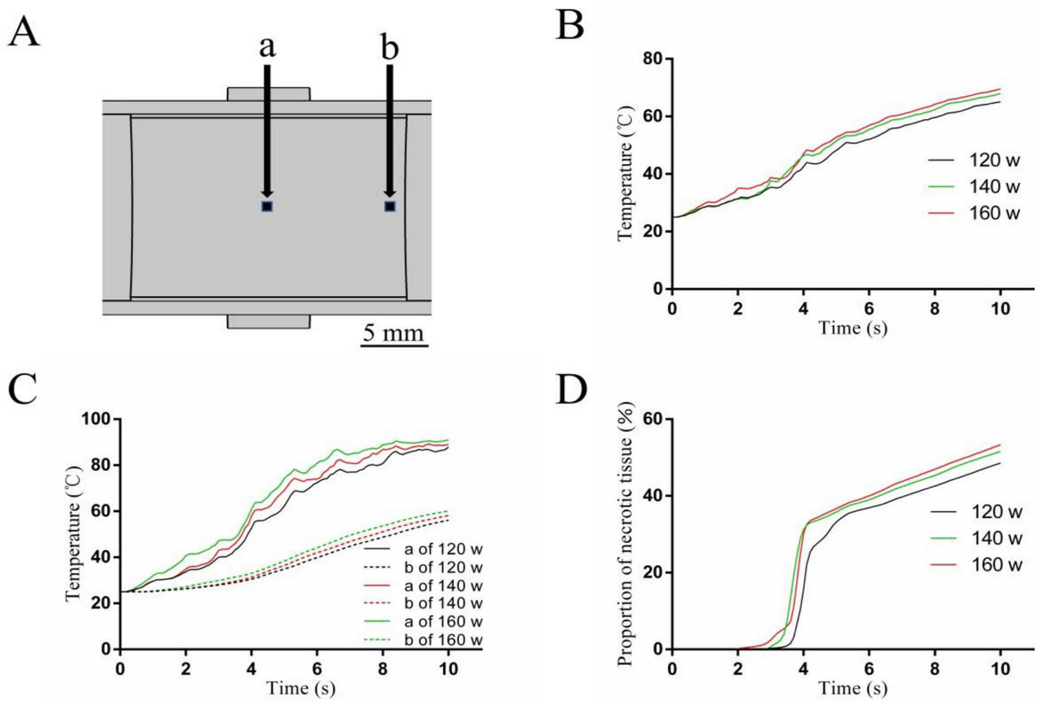

Figure 6. Changes in tissue temperature and proportion of necrotic tissue under three output powers. (A) Domain point location of T3 electrode; (B) Average temperature change of the welding area; (C) Temperature changes at domain points; (D) Proportion of necrotic tissue.

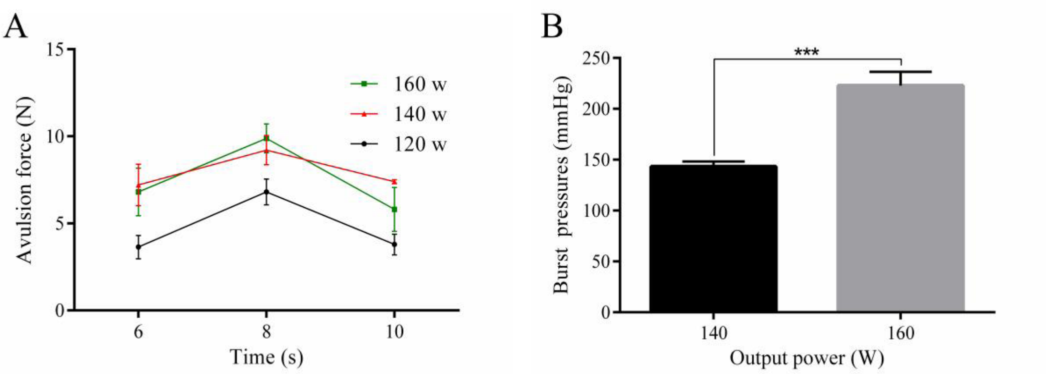

Figure 7. Biomechanical properties of anastomotic tissues under different welding parameters. (A) The avulsion force of the anastomotic tissue under different output powers (120 W, 140 W, 160 W) and different welding times (6 s, 8 s, 10 s); (B) The burst pressure of the anastomotic tissue at two output powers (140 W, 160 W) in 8-second welding time (***indicates a p value less than 0.001, indicating an extremely significant difference between the two sets of data).

as the experimental electrode. The results of the tear-off force are shown in **Figure 7A**. The tear-off force initially increased and then decreased as welding time extends, across all three output power levels. Notably, at an output power of 120 W and a welding time of 6 seconds, the tear-off force reached its minimum value of 3.64±0.67 N, suggesting that the anastomosis may fail under lower output power and shorter welding durations. In contrast, at an output power of 160 W and a welding time of 8 seconds, the tear-off force reached its maximum value of 9.87±0.83 N. The results of the Student's t-test indicated no significant difference in the tear-off force at output powers of 140 W and 160 W after 8 seconds of welding (P=0.38). Therefore, further burst pressure experiments would be conducted to determine the optimal output power for welding parameters.

Intestinal tissue welding experiments were conducted at two output power levels, and the burst pressure results are shown in **Figure 7B**. The welding time was fixed at 8 seconds. At an output power of 140 W, the burstpressure was

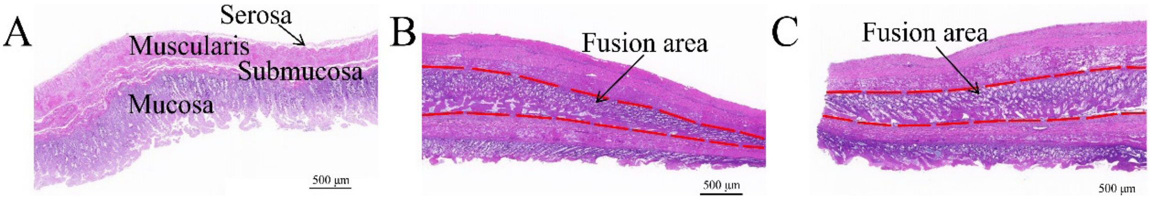

Figure 8. Histopathological examination of the anastomotic area. (A) Normal intestinal tissue; (B) Anastomosis area at 140 W power; (C) Anastomosis area at 160 W power.

143.31±5.02 mmHg, while at 160 W, the burst pressure increased to 222.88±13.48 mmHg. Clinically, the highest intra-abdominal pressure typically ranges from 100 to 150 mmHg [25]. The results indicate that only at an output power of 160 W did the burst pressure exceed the maximum intra-abdominal pressure. Therefore, an output power of 160 W and a welding time of 8 seconds were selected as the optimal welding parameters.

Histopathological examination

Figure 8 presents histopathological images of normal intestinal tissue and the anastomosis site under two magnifications, with a compression force of 20 N and a welding time of 8 seconds. The distinct separation of the serosa, muscular layer, submucosa, and mucosa was clearly visible in normal intestinal tissue. In contrast, the anastomosis area following welding exhibited a reduced thickness of the two intestinal layers, with a tightly fused connection, suggesting enhanced tissue union under the applied welding conditions. At an output power of 140 W, the anastomosis area displayed an uneven structure, with regions ranging from loose to dense, increasing the likelihood of leakage under the peristaltic forces of the intestine. However, at an output power of 160 W, the anastomosis demonstrated a more uniform thickness with a stable and secure connection, indicating more reliable tissue fusion.

Discussion

Colorectal cancer is a common malignancy of the digestive tract. Clinically, after surgical resection, the remaining tissue is typically reconnected using manual suturing or stapler anastomosis. However, both methods are associated with complications such as bleeding and anastomotic fistula formation. To address these challenges, tissue welding technology utilizing radiofrequency energy has been proposed as an innovative approach for tissue anastomosis. This technique leverages the thermal effects on tissue to achieve rapid and secure anastomosis without the need for foreign materials, offering distinct advantages over traditional methods.

Biodegradable magnesium alloys present a novel approach to tissue welding electrode design. Unlike traditional materials, magnesium alloy electrodes do not require removal through secondary surgery after completing tissue anastomosis, minimizing tissue damage. Mao et al. developed welding electrode structures using magnesium alloys, demonstrating improved welding strength while maintaining safety [15]. However, their study did not investigate the effects of electrode weight and mechanical support in depth. Therefore, this study focuses on electrode thickness and explores the potential for weight reduction while preserving mechanical strength.

First, mechanical simulations were conducted on the three types of circular electrodes. The results indicated that, under a force of 20 N, both the stress and strain experienced by the electrodes gradually decreased with increasing thickness. This suggests that a greater thickness reduces the likelihood of plastic deformation and stress concentration. Conversely, if the electrode is too thin, it may fail to provide effective support, potentially leading to anastomosis failure. Therefore, it is essential to identify a thickness that balances mechanical requirements with the need to reduce electrode weight based on material characteristics.

In our study, the maximum deformation of the T3 electrode was measured at 0.23194 mm, with a corresponding maximum strain of 1.2% and maximum stress of 122.26 MPa. These values fell within the elongation and yield strength range of WE43 magnesium alloy, indicating that this electrode meets the mechanical requirements for operational use. In contrast, the other two electrodes exceeded the material's yield strength, posing a risk of plastic deformation. Thus, an optimal thickness of 0.4 mm was selected for the electrodes.

Finite element analysis was conducted to examine the temperature distribution and thermal damage of the anastomotic tissue at three different power levels: 120 W, 140 W, and 160 W. The results showed that the minimum average maximum temperature of the tissue was 65.1 °C, while the maximum was 69.6 °C. The minimum average maximum thermal damage was 48.6%, and the maximum was 53.3%. These findings indicate that, under the same mechanical pressure and welding time, increasing power has a minimal effect on the average thermal damage to the tissue. The temperature differences observed at key points, labeled a and b, may be attributed to their positions relative to the welding area. Point a is located within the welding area, where the welding power directly influences the region, causing a rapid temperature increase. In contrast, point b is situated outside the welding area, where heat is transmitted through the electrode, leading to heat dissipation. As a result, the temperature increase at point b lags behind that at point a, and the temperature remains lower.

Mechanical pressure, output power, and welding time collectively influence the effectiveness of anastomosis. Research indicates that a pressure of 20 N is acceptable for tissue during welding. However, due to variations in electrode structure and materials, it is crucial to determine the optimal welding parameters, including output power and welding time, in this study. During normal intestinal function, peristalsis occurs. If the anastomotic tissue is not adequately adhered, there is a risk of anastomotic leakage. Effective anastomosis can only be achieved if it can withstand intestinal peristalsis.

Common methods for evaluating welding effectiveness include the avulsion force test and burst pressure test. The welding outcome is assessed by comparing the maximum tensile force at which the anastomosis fails during stretching with the maximum pressure at which leakage occurs during perfusion. Generally, an avulsion force exceeding 6 N and a burst pressure greater than 30 mmHg are considered necessary for successful anastomosis [26]. In our study, with an output power of 160 W and a welding time of 8 seconds, the avulsion force reached a maximum of 9.87±0.83 N, and the burst pressure was recorded at 222.88±13.48 mmHg. Additionally, histopathological examination revealed a uniform thickness of the anastomotic area with a stable connection, which adequately met the mechanical requirements for the intestine under normal physiological conditions.

In conclusion, we designed three different thicknesses of circular electrodes to reduce the electrode weight. Finite element analysis revealed that a thickness of 0.4 mm satisfies the mechanical requirements for the welding process. In vitro tissue welding experiments, including tearing force, burst pressure tests, and tissue pathology assessments, were conducted to evaluate the performance of the electrodes. The results demonstrated that the optimal welding parameters were 8 seconds of welding time and 160 W of output power, yielding an average tearing force of 9.87±0.83 N and an average burst pressure of 222.88±13.48 mmHg.

We have investigated the optimal electrode thickness from a mechanical perspective. However, the in vivo corrosion behavior of magnesium alloy-based implanted electrodes requires further experimental investigation. Additional research is needed before these electrodes can be fully considered for clinical application.

Author contributions: Lin Mao and Juxiao Wang conceived this project. Lin Mao and Juxiao Wang were responsible for the structural design and finite element simulation. Lin Mao and Chengli Song designed the intestinal welding experiment and anastomotic strength testing experiment. Juxiao Wang and Weiwei Fan conducted the experiments, collected relevant data, and performed the analysis. All authors contributed to the writing of the manuscript.

References

[1] Dekker E, Tanis PJ, Vleugels JLA, et al. Colorectal cancer. Lancet 2019;394(10207):1467–1480.
[2] Zhou H, Wang W, Luo P, et al. Trend of Colorectal Cancer Burden in China from 1990 to 2019. Cancer Res Prev Treat 2024;51(2):115–120.
[3] Akgül Ö, Çetinkaya E, Ersöz Ş, et al. Role of surgery in colorectal cancer liver metastases. World J Gastroenterol 2014;20(20):6113–6122.
[4] Breitenstein S, Rickenbacher A, Berdajs D, et al. Systematic evaluation of surgical strategies for acute malignant left-sided colonic obstruction. Br J Surg 2007;94(12):1451–1460.
[5] Han S, Cai Z, Ning X, et al. Comparison of a New High-Frequency Electric Welding System for Intestinal Closure with Hand-Sewn In Vivo Pig Model. J Laparoendosc Adv Surg Tech A 2015;25(8):662–667.
[6] Kramer EA, Rentschler ME. Energy-Based Tissue Fusion for Sutureless Closure: Applications, Mechanisms, and Potential for Functional Recovery. Annu Rev Biomed Eng 2018;20:1–20.
[7] Santini M, Fiorelli A, Messina G, et al. Use of the LigaSure device and the Stapler for

closure of the small bowel: a comparative ex vivo study. Surg Today 2013;43(7):787–793.
[8] Tu L, Zhou Y, Song C, et al. Preliminary study of a control algorithm for radio-frequency-induced intestinal tissue fusion. Int J Hyperthermia 2019;36(1):1297–1306.
[9] Wootten S, Zawacki ZE, Rheins L, et al. An evaluation of electrocoagulation and thermal diffusion following radiofrequency microneedling using an in vivo porcine skin model. J Cosmet Dermatol 2021;20(4):1133–1139.
[10] Elzayat S, Elsherif H, Aouf M. Trans-oral endoscopic assisted radio-frequency for adenoid ablation; A randomized prospective comparative clinical study. Auris Nasus Larynx 2021;48(4):710–717.
[11] Hu Z, Zong N, Song C, et al. Intestinal tissue fusion based on radiofrequency energy. J Med Biomech 2021;36:790-796.
[12] Holmer C, Winter H, Kröger M, et al. Bipolar radiofrequency-induced thermofusion of intestinal anastomoses--feasibility of a new anastomosis technique in porcine and rat colon. Langenbecks Arch Surg 2011;396(4):529-533.
[13] Zhao L, Song C, Wang Z, et al. Novel concave-convex electrode for colonic anastomoses by radiofrequency thermo-fusion. Surg Endosc 2015;29(7):1809-1816.
[14] Zong NX, Hu ZX, Xing XP, et al. Innovative Design and Experimental Study of Degradable Radiofrequency Energy Tissue Welding Electrodes. Model Sim 2022;11(2):454-464.
[15] Mao L, Han Z, Xing X, et al. Development of implantable electrode based on bioresorbable Mg alloy for tissue welding application. Sci Rep 2024;14(1):16110.
[16] Petter-Puchner AH, Fortelny RH, Walder N, et al. Small intestine submucosa (SIS) implants in experimental IPOM repair. J Surg Res 2010;161(2):264-271.
[17] Woźniak-Budych MJ, Staszak K, Staszak M. Copper and Copper-Based Nanoparticles in Medicine-Perspectives and Challenges. Molecules 2023;28(18):6687.
[18] Jiang HS, Zheng MY, Qiao XG, et al. Microstructure and mechanical properties of WE43 magnesium alloy fabricated by direct-chill casting. Mater Sci Eng: A 2017;684:158-164.
[19] Li S, Yang X, Hou J, et al. A review on thermal conductivity of magnesium and its alloys. J Magnes Alloys 2020;8(1):78-90.
[20] Eivani AR, Tabatabaei F, Khavandi AR, et al. The effect of addition of hardystonite on the strength, ductility and corrosion resistance of WE43 magnesium alloy. J Mater Res Technol 2021;13:1855-1865.
[21] Byun SH, Lim HK, Cheon KH, et al. Biodegradable magnesium alloy (WE43) in bone-fixation plate and screw. J Biomed Mater Res B Appl Biomater 2020;108(6):2505-2512.
[22] Xing X, Song C. A novel electrode to achieve balance between anastomotic strength and tissue thermal damage for radiofrequency-induced intestinal anastomosis. Acta Bioeng Biomech 2023;25:3-13.
[23] Arya S, Hadjievangelou N, Lei S, et al. Radiofrequency-induced small bowel thermofusion: an ex vivo study of intestinal seal adequacy using mechanical and imaging modalities. Surg Endosc 2013;27(9):3485-3496.
[24] Kubásek J, Dvorskỳ D, Čavojský M, et al. WE43 magnesium alloy – material for challenging applications. Met Mater 2019;57:159-165.
[25] Deprest J, Zheng F, Konstantinovic M, et al. The biology behind fascial defects and the use of implants in pelvic organ prolapse repair. Int Urogynecol J 2006;17(1):16-25.
[26] Xing X, Song C. A novel electrode for reducing tissue thermal damage in radiofrequency-induced intestinal anastomosis. Minim Invasive Ther Allied Technol 2024;33(2):80-89.